Innovative use of passive and active distributed temperature sensing for estimating infiltration rates in a managed aquifer recharge framework

Robin Glaude[a], Nataline Simon[a,b], Serge Brouyère[a]

[a] University of Liège, Urban and Environmental Engineering, Hydrogeology and Environmental Geology, Belgium

[b] Université Gustave Eiffel, COSYS, IMSE, 77420 Champs-sur-Marne, France

Corresponding author: Robin Glaude (robin.glaude@uliege.be)

Abstract

Managed Aquifer Recharge (MAR) has become an essential strategy for sustainable water management. Effective design of surface recharge systems relies on the accurate estimation of the soil infiltration capacity. In this context, the use of heat as a tracer has recently gained attention to quantify infiltration dynamics. Particularly, methods relying on Distributed Temperature Sensing (DTS) along fiber optic (FO) cables have been developed to account for the spatial variability of the recharge. This study explores an innovative approach that combines two types of temperature sensing techniques, passive and active-DTS measurements, to evaluate infiltration rates in a MAR pilot site. An FO cable, buried in the loess sediments of an infiltration basin, recorded temperature changes during an infiltration test. First, the passive method monitored natural temperature changes as cooler water filled the basin, enabling the estimation of initial infiltration rates. Twenty-four hours later, the active method involved heating part of the cable to further assess infiltration rates during ongoing infiltration. The analysis of DTS data facilitated the mapping of the recharge within the MAR system. Furthermore, results show that the infiltration rate is significantly higher at the start of the infiltration test, demonstrating that combining passive and active-DTS measurements provides a better understanding of the infiltration dynamics. The findings demonstrate the viability of MAR in loess-based systems at the studied site and highlight the potential of DTS methods for long-term monitoring of MAR operations.

Keywords: Managed Aquifer Recharge (MAR); Distributed Temperature Sensing (DTS); Infiltration monitoring; Recharge mapping; Heated Fiber Optic Cable; Heat tracer experiment

1. Introduction

Groundwater availability and sustainability are threatened by climate change and anthropogenic pressure (Green *et al.*, 2011). The Intergovernmental Panel on Climate Change (IPCC) predicts an increase in the global mean temperature, which would directly impact the hydrological cycle by increasing surface water evaporation rates, enhancing vegetation transpiration, and altering precipitation patterns (Calvin *et al.*, 2023). These changes are anticipated to result in a long-term decline in groundwater availability. Concurrently, water demand is expected to increase, particularly during peak periods such as summer months (Boretti and Rosa, 2019; Wu *et al.*, 2020). In this context, Managed Aquifer Recharge (MAR) emerges as an adaptive strategy to address disparities between groundwater supply and water demand. MAR is defined as “the purposeful recharge of water to

aquifers for subsequent recovery or environmental benefit“ (Dillon, 2009) and is an essential component of sustainable water resource management, as it enhances subsurface water storage (Dillon, 2005; Page *et al.*, 2018). As water is filtered through soil during recharge, MAR also ensures the long-term availability of clean and reliable water sources for various applications (Amy and Drewes, 2007; Sharma and Kennedy, 2017; Sprenger *et al.*, 2017).

Effective design of surface recharge systems relies on the accurate estimation of soil infiltration capacity to assess the permeability of the vadose zone (Bouwer et al., 2008). Soil infiltration capacity is a critical parameter for the deployment of MAR (Maliva, 2015; Prathapar *et al.*, 2015) and is strongly influenced by soil texture, one of the primary factors governing its ability to infiltrate water into the subsurface (Singh *et al.*, 2013; Bonilla Valverde *et al.*, 2016). Coarse soils, such as sands or gravels, typically facilitate drainage of water due to their larger and more interconnected pore spaces, resulting in higher permeability. Conversely, soils with fine pores or high clay content (>10%), such as loamy soils, often have lower permeability and infiltration capacity due to less connected pores, restricting water movement. Consequently, these soils are generally excluded from MAR design due to their reduced capacity to transmit water effectively (Bouwer, 2002; Kallali *et al.*, 2007). Nevertheless, implementing surface spreading MAR systems for aquifers overlaid by low to moderate permeability soils can still be beneficial. The low permeability layer can enhance water purification by acting as a natural filter, removing contaminants, and improving water quality as it percolates through the soil (Nadav *et al.*, 2012; Sharma and Kennedy, 2017). Moreover, in regions where high-permeability soils are limited and low-permeability soils prevail, this approach may be the only viable option. Although infiltration rates are slower than in high-permeability soils, spreading the recharge over a larger surface area can still result in effective aquifer replenishment.

Traditional methods to measure infiltration rates often use cylinder infiltrometers, such as single-ring or double-ring infiltrometers. A double-ring infiltrometer consists of two concentric metal cylinders. Water is poured into both cylinders, and the infiltration rate is measured in the inner ring, with the outer ring minimizing lateral flow. This method provides useful local estimates of infiltration rates but may overestimate the infiltration rate due to lateral water flow beneath the infiltrometer (Bouwer, 1986).

Innovative methods, such as using heat as a tracer, overcome this limitation and allow for a more comprehensive estimation of infiltration rates on a larger spatial scale. For instance, Caligaris *et al.* (2022) used heat as a tracer to assess the recharge plume in a MAR system. They monitored temperature data using sensors installed at various depths in wells near the MAR site. This approach underscored the interest of monitoring temperature variations in groundwater to gain a better understanding of dynamic subsurface water movements. Other studies on heat experiments in the context of MAR (Pidlisecky and Knight, 2011; Racz *et al.*, 2012) have successfully quantified infiltration rates. However, these studies also emphasize that infiltration rates vary over time and space, highlighting the need for methods that can characterize the spatial and temporal variabilities of this critical parameter.

In this context, the use of Distributed Temperature Sensing (DTS) technology, which provides distributed temperature measurements at high resolution along a Fiber Optic (FO) cable, is of particular interest. Racz *et al.* (2012), Becker *et al.* (2013), and Mawer *et al.* (2016) employed DTS to estimate infiltration rates in recharge basins and infiltration ponds. The DTS measurements facilitated the estimation of infiltration rates over both time and space by analyzing diurnal temperature

fluctuations recorded along buried FO cables, which are induced by the propagation of air temperature changes at depth. It is important to note that the term “passive-DTS” measurements is frequently employed to describe natural temperature fluctuations.

While passive-DTS measurements are useful for characterizing infiltration rate variabilities, they face limitations such as low thermal response sensitivity at very low infiltration rates and dependence on natural temperature fluctuations (Gilmore *et al.*, 2019; Le Lay *et al.*, 2019; Koruk *et al.*, 2020; Simon *et al.*, 2022). Conversely, active-DTS methods introduce an artificial heat source by injecting electricity through the steel armoring of the FO cable. This allows for controlled heating and measurement of the thermal response (Read *et al.*, 2014; Bense *et al.*, 2016). This approach provides high spatial resolution estimates of groundwater flux, independent of natural temperature variations (Simon *et al.*, 2021). Although active-DTS has been successfully applied in streams (Simon *et al.*, 2022, 2024; Sai Louie *et al.*, 2023), its potential for exploring recharge variability in MAR systems remains unexplored.

The implementation of active-DTS within MAR framework has the potential to significantly improve recharge monitoring, as it provides measurements that are independent of natural temperature fluctuations. This makes it a more reliable and flexible option, enhancing the accuracy and applicability for MAR assessment. The objective of this study is to demonstrate the effectiveness of DTS technology. To that end, the study quantifies the spatial and temporal variability of recharge rates. This is accomplished by integrating both active and passive-DTS measurements along a FO cable during an infiltration test. Furthermore, this study investigates the temporal dynamics of infiltration in low-permeability sediments by interpreting DTS data at different stages of the test. This approach aims to evaluate the feasibility and benefits of MAR applications in soils with low to moderate permeability. The infiltration test was conducted in a small infiltration basin located above the Hesbaye chalk aquifer (Belgium). The FO cable was buried in loess sediments at the base of the basin to collect DTS data throughout the experiment.

2. Materials and Methods

2.1. Experimental site

The Geer hydrological basin is located northwest of the city of Liège, in Belgium, and overlays the Hesbaye chalk aquifer, one of the most significant groundwater bodies in Wallonia. The aquifer supplies approximately 15 million cubic meters of water annually to the city of Liège through pumping wells and drainage galleries (Orban *et al.*, 2014; CILE, 2022). However, this major aquifer is facing threats to its quantity and quality (Hakoun *et al.*, 2017). A significant decline in groundwater levels has been documented, with a 6-meter reduction observed between 1990-2020 compared to 1960-1990 (Goderniaux *et al.*, 2023). This trend is largely attributed to climate change, which has altered precipitation patterns and increased evapotranspiration, reducing recharge efficiency and increasing the aquifer's susceptibility to long-term depletion. Specifically, Goderniaux *et al.* (2023) reported a decrease in mean annual recharge from 207 $mm \cdot yr^{-1}$ in 1960-1990 to 117 $mm \cdot yr^{-1}$ in 1990-2020, underscoring the importance of managed aquifer recharge strategies in the region. MAR has thus been identified as a promising mitigation approach to enhance subsurface storage and maintain groundwater availability in the region.

The Geer hydrological basin is primarily composed of Quaternary loess (eolian loamy sediments), which can reach up to 20 m in thickness and cover the chalk aquifer (Batlle Aguilar *et al.*, 2007). This loess layer is characterized by moderate hydraulic conductivity, around 10^{-7} $m \cdot s^{-1}$ (Brouyère, 2001).

Due to the low permeability of this layer, the implementation of MAR may be challenging in this area, as the reduced infiltration capacity can limit the rate at which water can be introduced into the aquifer. MAR applications in loess environments are not frequently documented. This underscores the necessity for site-specific assessments to evaluate their feasibility in such geological settings.

In this context, a pre-existing sedimentation basin connected to a production well was selected as a pilot site for investigating recharge processes occurring through the loess. The basin's truncated pyramid shape (see Figure *1*) ensures uniform distribution of water over a large surface area, facilitating effective infiltration. The base of the structure consists of a 30-centimeter layer of cobblestone, which overlays loess sediments. The basin's concrete sides offer structural stability and prevent lateral leakage. The basin is connected to a pumping well through a steel pipe that enables the filling of the basin with a flow rate of around 15 $m^3 \cdot h^{-1}$. Drilling data in the area revealed a layer of loess ranging from 7.25 to 11.5 meters in thickness beneath the surface, succeeded by an 8-meter layer of silt and flint conglomerate before encountering a chalk layer approximately 35 meters thick.

Figure 1. Infiltration basin during a) the installation of the FO cable and b) its replenishment.

2.2. Experimental configuration

DTS measurements were conducted using a 3.8 mm diameter FO cable (4 multimode 50/125-µm fibers). The cable was arranged in a U-shape in the basin (see Figure 2) and buried within the loess sediments at a depth of approximately 10 centimeters. Within the buried section measuring 17.5 meters, 7.5 meters were electrically connected to a Heat Pulse Control System (see Figure 2). This system was used to inject electricity into the electric cables/FO cable system for active-DTS measurements.

DTS measurements were conducted using an AP Sensing interrogator instrument (DTS N4386B), which provided temperature records every 25 centimeters along the FO cable with a 10-second sampling interval. The data were calibrated using two calibration baths: one cold bath filled with ice and water and one warm bath with heated water using a heating resistor. Approximately 10 meters of FO cable section were immersed in the calibration baths (see Figure 2). Temperature sensors (PT100) with 0.1°C accuracy were also submerged in the calibration baths for data calibration. The interrogator was configured using an enhanced version of the single-end configuration (Hausner *et al.*, 2011), as two

sections of the FO cable were placed in the cold calibration bath. This configuration enabled verification that signal attenuation along the FO cable was negligible. The use of calibration baths ensured high-quality measurements along the entire cable.

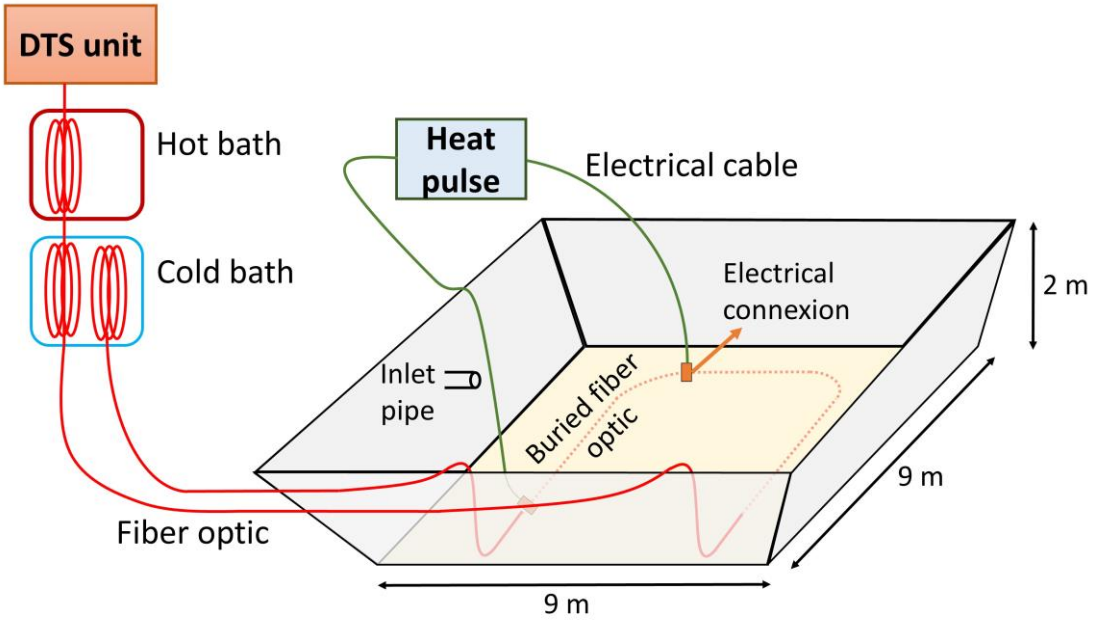

Figure 2. DTS configuration. Please note that this schematic excludes the cobblestone layer. The continuous red line indicates the FO cable, which is not buried, while the dashed red line delineates the buried section of the FO cable. The heated section of the FO cable is comprised between the two electrical connections.

One pressure sensor (CTD diver type) was buried within the cobblestone layer to monitor water pressure evolution during the infiltration test. The data acquisition process was programmed with a five-minute sampling interval. These data were used to obtain a comprehensive estimate of the infiltration rate for the entire basin over time, enabling a comparison and validation of infiltration rate estimates obtained through passive and active-DTS analysis.

2.3. Active and passive-DTS measurements

The infiltration test was conducted at the end of July 2023. The basin was initially empty and subsequently filled with water for a period of seven hours (see Figure 3). Passive-DTS measurements were continuously recorded to monitor natural temperature variations along the entire FO cable throughout the entire experiment. These measurements captured soil temperature before, during, and after the basin replenishment. Since the water used to fill the basin was 14°C, colder than the initial sediment temperature of 16 °C, a decrease in soil temperature was expected as the cooler water reached the FO cable. The resulting temperature changes were used to estimate the infiltration rate at the onset of the infiltration test. This approach is particularly useful for assessing initial infiltration dynamics, offering valuable insights into the early stages of water movement through the subsurface. Furthermore, passive-DTS measurements can be interpreted along the entire length of the FO cable, providing a comprehensive view of the infiltration process beyond the heated section. This enhances the overall understanding of the infiltration dynamics within the basin.

The active-DTS experiment was initiated 24 hours after the start of the basin replenishment (see Figure 3) and involved heating a segment of the FO cable. The section of cable connected to the heat pulse

(7.5 meters) was heated for a duration of 9 hours and 30 minutes by injecting a constant electrical current of 17.98 $W.m^{-1}$. Active-DTS measurements were analyzed to estimate the infiltration rate 24 hours after the infiltration test began, as well as the thermal conductivity of the soil surrounding the FO cable. The thermal conductivity values derived from active-DTS measurements served as inputs for the heat transfer finite element numerical model to interpret passive-DTS data. Therefore, this section first presents the methodology for interpreting active-DTS, as it provides essential thermal properties required for the analysis of passive-DTS measurements. Subsequently, the interpretation of passive-DTS data is detailed.

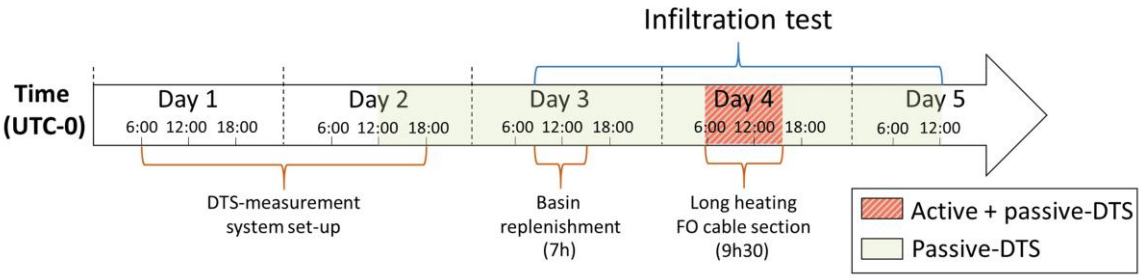

Figure 3. Schedule of the experiment.

2.3.1. Interpretation of Active-DTS measurements

The use of heated FO cables in saturated porous media to estimate water flux has been investigated in several studies (Des Tombe *et al.*, 2019; Del Val *et al.*, 2021; Simon *et al.*, 2021). Active-DTS involves the use of an artificial heat source, caused by electrical current injection, and the subsequent monitoring of the induced temperature increase (ΔT) over time. During the initial heating phase, the temperature increase is primarily driven by heat conduction and storage within the FO cable. Heat storage within the cable leads to a significant temperature increase (ΔT_{FO}) (Del Val *et al.*, 2021; Simon *et al.*, 2021).

Once the heat begins to propagate into the surrounding porous media, conduction and advection are the two primary heat transfer processes that control the temperature evolution. Conduction refers to the transfer of heat through direct contact between solid grains in the porous media, while advection involves the transfer of heat due to the movement of the water, as defined by Anderson (2005). Initially, the temperature increase is governed by conduction, which depends on the thermal conductivity of the porous media. During this stage, a continuous and gradual temperature increase is observed over time on a semi logarithmic plot. Consequently, the thermal conductivity (λ) can be estimated by analyzing the thermal response measured during this phase. Subsequently, the heat is dissipated by advection due to the groundwater flux (q). Advection processes, which depend on flow conditions, are responsible for temperature stabilization at later times of heating. High water fluxes facilitate greater heat dissipation through advection, resulting in lower temperature increases. Conversely, lower water fluxes result in reduced heat dissipation, leading to greater temperature increases (Simon *et al.*, 2021).

Active-DTS measurements were interpreted using the ADTS toolbox proposed by Simon and Bour (2023). The ADTS toolbox employs a mathematical model referred to as the Moving Instantaneously Line Source (MILS) to simulate the temporal variations in temperature resulting from the movement of heat through the porous media (Simon *et al.*, 2021). The MILS model conceptualizes the heat source

as an infinite line that instantaneously releases heat, thereby enabling the analysis of the subsequent heat dispersion through the surrounding medium. It facilitates the automatic interpretation of each measurement point along the heated section of the FO cable, providing estimates of both the sediment thermal conductivity and groundwater flux. This approach offers two key advantages. First, it enables the direct and spatially distributed estimation of groundwater flux without relying on hydraulic conductivity values, which are often uncertain, point-based, and not representative of the study scale. Secondly, while thermal conductivity is necessary for accurately interpreting the thermal response along the FO cable, its spatial variability also provides valuable insights into subsurface heterogeneity.

The ADTS Toolbox employs a two-step process to interpret thermal response curves measured during the heating phase. After evaluating the early-stage temperature increase (ΔT_{FO}) within the FO cable, the first step consists in estimating the thermal conductivity (λ) of the porous media by analyzing the thermal response along the heated FO cable during the conduction-dominant period. The linear increase in temperature (ΔT) observed on a semi-logarithmic plot during the conduction-dominated phase is governed solely by thermal conduction and is not influenced by advective flow (q). This behavior is modeled using the MILS analytical solution with a flow velocity q = 0 m·s^{-1}, allowing for the determination of λ. In the second step , the temperature stabilization observed during the advection-dominant period is reproduced using the MILS model by adjusting the groundwater flux q, providing a reliable estimate of local infiltration rate.

To interpret active-DTS measurements, it is essential to consider natural temperature variations that may occur during the heating period. In their study, *Simon et al.* (2024) demonstrated that the temperature signal recorded during heating is a combination of the natural temperature variations and the induced temperature variations resulting from artificial heat injection. Natural temperature variations may result from the propagation in depth of diurnal temperature fluctuations in case of downward water fluxes controlling advective heat transport (Constantz, 2008a). Given the extended heating period (9.5 hours), it is anticipated that ambient temperature variations may also occur during the heating process. The methodology proposed by *Simon et al.* (2024) to remove ambient temperature variations from the signal was therefore applied. The process entails identifying a *"matching point"* for each measurement along the heated section of the FO cable. The matching point is a location along the non-heated section where similar temperature fluctuations are expected to be measured as along the heated section. After identifying the matching point, a corrective adjustment is applied to the heated section's data. This adjustment involves subtracting the temperature recorded at the matching point from the temperature recorded at the associated heated section's measurement point. This procedure ensures that the remaining temperature variations exclusively reflect variations induced by the heat injection.

2.3.2. Interpretation of Passive-DTS measurements

The passive-DTS measurements recorded during the infiltration basin's replenishment were interpreted using a finite element heat transfer numerical model with fluid flow (see Figure *4*). The model was developed with the "heat transfer in porous media" module of COMSOL Multiphysics ® (COMSOL, 2024). It simulates temperature variations in loess caused by the infiltration of cooler water. A 2D vertical model was adopted, assuming that water flow predominantly occurs in the vertical direction with minimal lateral variation. This assumption is supported by the shallow burial depth of the FO cable (Kurylyk *et al.*, 2017) and the predominance of advective over conductive heat transport under these conditions, as further detailed in Section 4.1. Consequently, both heat advection and

conduction are expected to occur along the vertical dimension only, as the infiltration basin uniformly distributes water across its surface. The numerical modeling approach was selected over analytical solutions, as it enables the simulation of coupled heat and water flow processes that are too complex to be captured analytically.

The model dimensions are 50 × 20 cm along the vertical and horizontal axes, respectively. The model's finite element grid consists of thin triangular elements with sides of approximately 1.85 cm (see Figure 4). This element size has been selected to ensure numerical stability, with a Courant number calculation (C = 0.5) confirming that the time step and mesh resolution used result in a stable solution (see Section S1 of the supplementary materials). The initial temperature values assigned to the entire model correspond to the soil temperature before the infiltration began, ranging from 15.41°C to 16.71°C. A constant temperature is applied at the top of the model, set to the average stabilized water temperature following basin replenishment (ranging from 13.57°C to 14.39°C). This average is computed over a stabilization period to mitigate thermal noise. The constant temperature of the basin water reflects the rapid thermal equilibrium, driven by continuous replenishment, providing the model with stable thermal input. This constant temperature is coupled with a constant prescribed water flux, representing the infiltration rate. The bottom boundary is defined by a convection-dominated outflow, permitting heat loss solely through convection. The lateral boundaries are assigned a zero heat flux condition (0 $W \cdot m^{-1} \cdot K^{-1}$).

To estimate the infiltration rate, the prescribed flow in the model is adjusted until the simulated temperature at the FO cable depth (10 cm) closely aligns with passive-DTS observations. The best fit is obtained by minimizing the root mean square error (RMSE) between the observed and simulated thermal responses. Although a stationary flow is assumed, recharge may vary over time, especially at the start of the infiltration. This aspect is further explored through a comparison of constant and transient recharge models in Section 3.2.3. Model-derived infiltration rates were also compared with field measurements from a constant-head well permeameter conducted in loess sediments inside and outside the basin prior to the infiltration test (see Section S2 of the supplementary materials).

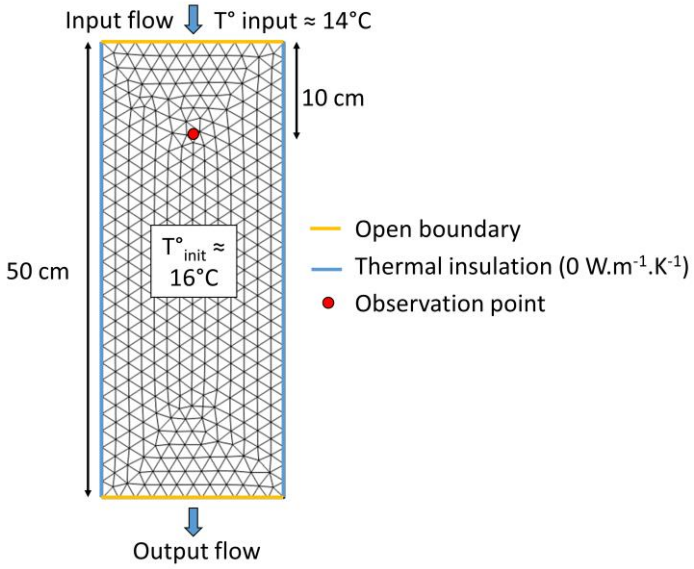

Figure 4. Heat transfer model implemented in COMSOL to interpret passive-DTS measurements.

Table 1 presents the physical and thermal properties of the loess sediments, water and saturated porous medium. Granulometry tests were carried out to estimate the bulk density and the porosity of the loess, using samples collected from the infiltration basin. The volumetric heat capacities of the saturated porous material and of the water were defined based on literature (Bilskie, 1994; Stauffer *et al.*, 2013; Khaled A and Nidal H, 2020). The mean thermal conductivity of the saturated sediments was estimated using active-DTS. Detailed explanations regarding the derivation of all properties listed in Table 1 are provided in the section S3 of the supplementary materials, including the distinction between the thermal properties of the saturated porous medium and those of the solid matrix, which were calculated using COMSOL-based equations.

Table 1. Input parameters for COMSOL software. 1 : measured; 2: from literature.

Property	**Unit**	**Saturated porous media**	**Liquid**	**Solid**
Thermal conductivity [1]	$W \cdot m^{-1} \cdot K^{-1}$	1.78	0.58	2.65
Density[1]	$Kg \cdot m^{-3}$	-	1000	2700
Volumetric Heat capacity at constant pressure[2]	$MJ \cdot m^{-3} \cdot K^{-1}$	3	4.1	2.2
Total porosity[1]	-	0.42	-	-

2.4. Transient infiltration rate modeling

The interpretation of passive-DTS measurements was conducted under the assumption of stationary flow conditions. However, as demonstrated by *Horton (1933, 1939)*, recharge decreases exponentially over time during infiltration. This decline can be attributed to several factors, including the swelling of colloids, the closing of soil cracks, the movement of fine particles into sediment pores, and soil packing due to increased water pressure. To address this phenomenon, new numerical simulations were conducted considering transient infiltration rates. Horton (1939) demonstrated that the evolution of the infiltration rate f at the beginning of the infiltration phase can be modeled using the following equation:

$$f = f_f + (f_0 - f_f) \times e^{-kt} \quad (1)$$

with f_0 the initial infiltration rate (capacity), f_f the final infiltration rate, k a constant related to soil properties and t the time from the beginning of the infiltration. The final infiltration rate f_f was estimated from pressure data at the end of the passive-DTS data interpretation period (after 21.92 hours), just prior to the collection of active-DTS data. Subsequently, the infiltration model (equation 1) was calibrated by adjusting both the initial infiltration capacity f_0 and the parameter k to reproduce the infiltration rate evolution derived from pressure data. To identify the optimal parameter set, an initial infiltration rate f_0 was prescribed, and the coefficient k was iteratively adjusted to minimize the RMSE between the modeled transient infiltration rate and the rate inferred from pressure data. For each optimal pair of f_0 and k, the transient infiltration model was implemented into COMSOL. The combination yielding the lowest RMSE between simulated and observed thermal responses was selected as the best fit.

2.5. Sensitivity analysis

Both passive and active-DTS analyses rely on assumptions that introduce uncertainties into the results. To assess the impact of critical parameters on these results, a sensitivity analysis was conducted. For active-DTS measurements, the proposed methodology has proven reliable (Simon *et al.*, 2022). The ADTS toolbox quantifies uncertainty related to instrumentation by assessing the impact of data noise on estimates of thermal conductivity and groundwater flux. It computes temperature increases over a range of thermal conductivity and flux values and derives associated uncertainties based on the system's temperature resolution (Des Tombe *et al.*, 2019; Simon and Bour, 2023).

For passive-DTS data interpretation, the sensitivity of the results depends on soil-related parameters introduced into the COMSOL model. In this study, we specifically examined the effects of thermal conductivity, volumetric heat capacity, and porosity on the model's output. Additionally, we investigated the impact of burial depth of the FO cable, as its exact positioning is subject to uncertainty and may influence the thermal response.

To assess how variations in these parameters impact the simulated thermal response, multiple models were tested by varying the values of each parameter. These models were then compared to a reference model, which was established using the parameters listed in Table 1 and the median infiltration rate inferred from passive-DTS analysis. The relative deviation is subsequently calculated using equation (2). This calculation indicates the degree to which the infiltration rate q_{model} diverges from the reference model rate q_{ref}. This analysis provides insight into the influence of both soil properties and FO burial depth on infiltration rate estimations.

$$relative\ deviation = \frac{q_{model} - q_{ref}}{q_{ref}} \times 100 \quad (2)$$

3. Results

The results are presented in two subsections. First, active-DTS data are interpreted using the MILS analytical model implemented within the ADTS toolbox. The analysis begins with the interpretation of the thermal response at a single point along the FO cable and is then extended to the entire heated section. Subsequently, passive-DTS data are analyzed using the COMSOL heat transfer numerical model. Similarly, the analysis starts at an individual location and is then generalized to the full extent of the buried FO cable. Note that full temperature profiles, recorded along the entire FO cable, are provided in the section S4 of the supplementary materials. These profiles show distinct thermal zones along the FO cable associated with calibration baths, surface exposure, and the buried section within the infiltration basin.

3.1. Active-DTS measurements

3.1.1. Thermal response interpretation

Figure 5 illustrates the two-step approach used to interpret the temperature increase recorded at a distance of 72.5 m along the FO cable, starting from the DTS unit. The first step entails reproducing the temperature increase that was measured during the conduction-dominant stage (see Figure 5a). Please note that during this stage, the heat propagation is primarily governed by conduction. This means that the temperature increase is exclusively dependent on the thermal conductivity of the porous media. This phase is observed between approximately 2 min 30 s and 5 h 20 min, during which a linear increase in the thermal response is observed. Among all the thermal conductivity values tested,

1.89 $W \cdot m^{-1} \cdot K^{-1}$ yielded the most accurate reproduction of the thermal response. The second step expands the interpretation to encompass the thermal response observed during both the conduction- and advection-dominant periods (see Figure 5b). At later times, a stabilization of the thermal response is observed due to heat dissipation by advection. The model shows that the infiltration rate of 4.16 × 10^{-6} $m \cdot s^{-1}$ leads to a temperature stabilization that aligns well with the observed data.

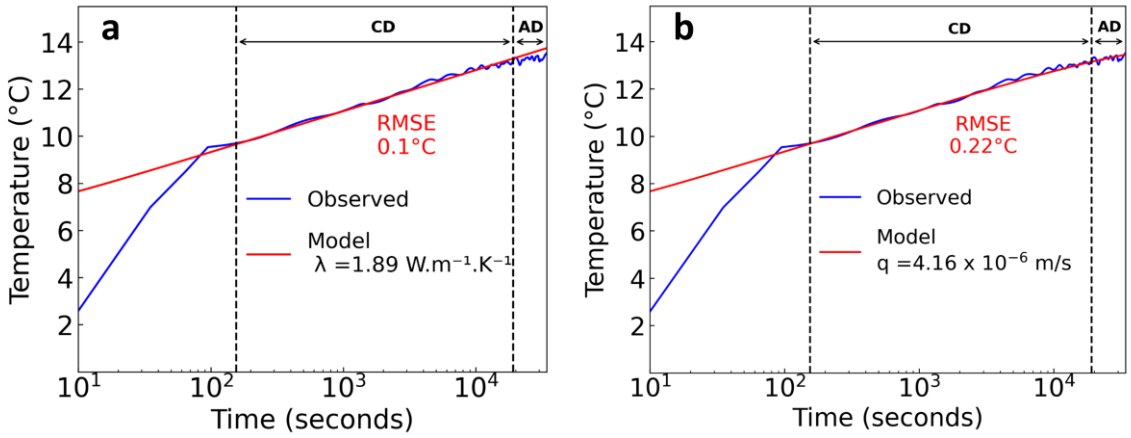

Figure 5. Thermal response recorded at 72.5 m from the DTS unit during the heating phase, along with the best-fit modeled curves obtained using the MILS model considering: a) only the conduction-dominant (CD) period, and b) both the conduction- and advection-dominant period (CD and AD). In both cases, ΔT_{FO} is set to 6.4°C.

3.1.2. Spatial variability of the infiltration rate along the heated FO cable section

The ADTS toolbox automatically implements the two-step interpretation previously introduced for each measurement point located along the heated section of the FO cable. It provides high-resolution estimates of both thermal conductivity and groundwater flux, facilitating the mapping of the thermal conductivities and infiltration rates within the basin sediments (see Figure 6a and b).

The results indicate that thermal conductivity values along the heated section range from 1.59 to 1.89 $W \cdot m^{-1} \cdot K^{-1}$, with an average of 1.78 $W \cdot m^{-1} \cdot K^{-1}$ (see Figure 6a). Given the spatial variability of thermal conductivity and the associated uncertainties in active-DTS interpretation using the ADTS toolbox (0.28 $W \cdot m^{-1} \cdot K^{-1}$), the total estimated range of thermal conductivity values is between 1.31 and 2.17 $W \cdot m^{-1} \cdot K^{-1}$. Laboratory measurements conducted on saturated loess samples collected from the infiltration basin yielded a thermal conductivity of 1.55 $W \cdot m^{-1} \cdot K^{-1}$, which is in good agreement with the DTS-based estimates. Additional details on the laboratory measurement are provided in Section S5 of the supplementary materials. A gradual increase in thermal conductivity is observed along the active section from the beginning to the end of the active section (point B to point C). Infiltration rates estimated along the heated section range from 2.01 × 10^{-6} $m \cdot s^{-1}$ and 4.69 × 10^{-6} $m \cdot s^{-1}$ (see Figure 6b), with a mean value of 3.79 × 10^{-6} $m \cdot s^{-1}$ (≈ 33 $cm \cdot day^{-1}$). As for the distribution of thermal conductivity values, infiltration rates also increase progressively from point B to point C.

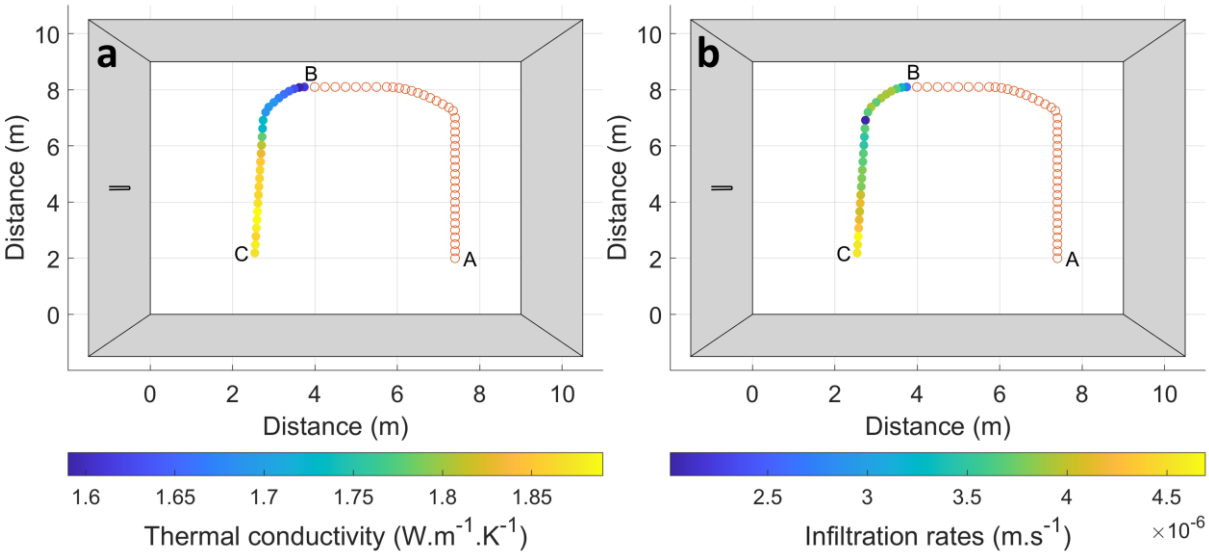

Figure 6. Maps of a) thermal conductivity and b) infiltration rate values derived from the interpretation of active-DTS data.

3.2. Passive-DTS measurements

3.2.1. Thermal decrease reproduction

The interpretation of passive-DTS measurements consists in reproducing the thermal response measured at the start of the basin replenishment with cold groundwater. Figure 7 illustrates an example of data interpretation for a single measurement point, located at a distance of 61 m along the FO cable, starting from the DTS unit. It appears that a recharge rate of 8.00×10^{-6} m·s^{-1} results in the best agreement between the model and the temperature measurements (RMSE = 0.06°C).

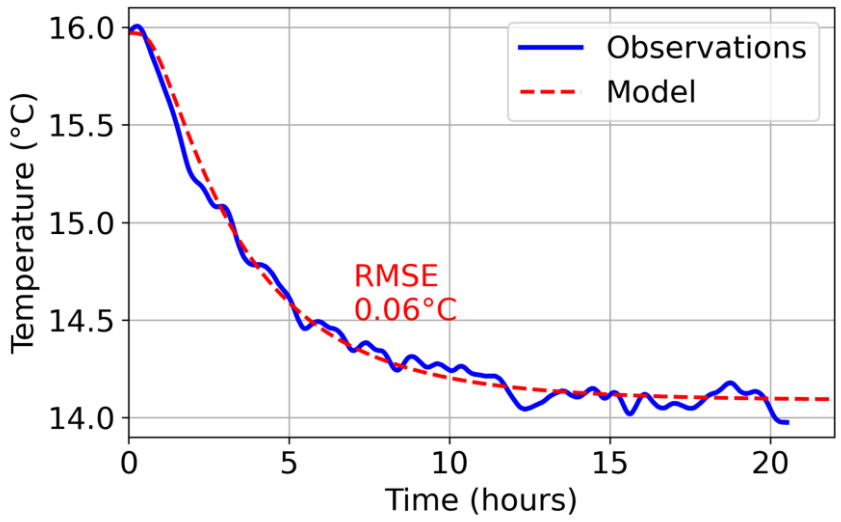

Figure 7. Thermal response model at 61 m along the FO cable from the DTS unit at the onset of the infiltration test.

3.2.2. Spatial variability of the initial infiltration rate along the FO cable

In contrast to the interpretation of active-DTS measurements, which permitted the estimation of infiltration rates exclusively along the heated section, the interpretation of passive-DTS measurements is applicable to any measurement point located along the buried section of the cable. Consequently, estimates of recharge rates can be obtained along the entire buried section (see Figure 8a). In

accordance with the results derived from active-DTS analysis, an increase in the recharge rate is observed from B to C (see Figure 8b), with infiltration rates ranging from 1.15 ×10^{-5} m·s^{-1} to 2.90 ×10^{-5} m·s^{-1}. Conversely, there is a gradual decrease in the recharge rate from B to A (see Figure 8a and b), with estimated infiltration rates ranging from 1.70 ×10^{-5} m·s^{-1} to 7.5×10^{-6} m·s^{-1}. The mean infiltration rate along the entire buried section of the FO cable is 1.51 ×10^{-5} m·s^{-1} (130 cm·day^{-1}). This value is in good agreement with field measurements obtained using a constant-head well permeameter, which ranged from 1.12 to 1.5 ×10^{-5} m·s^{-1}, thereby reinforcing confidence in the modeling results (see section S2 of the supplementary materials). RMSE values calculated between modeling results and field data range between 0.06 and 0.15°C, indicating a good fit of the models. The disparities in infiltration rates derived from the analysis of active- and passive-DTS data are addressed in the section 4.2.

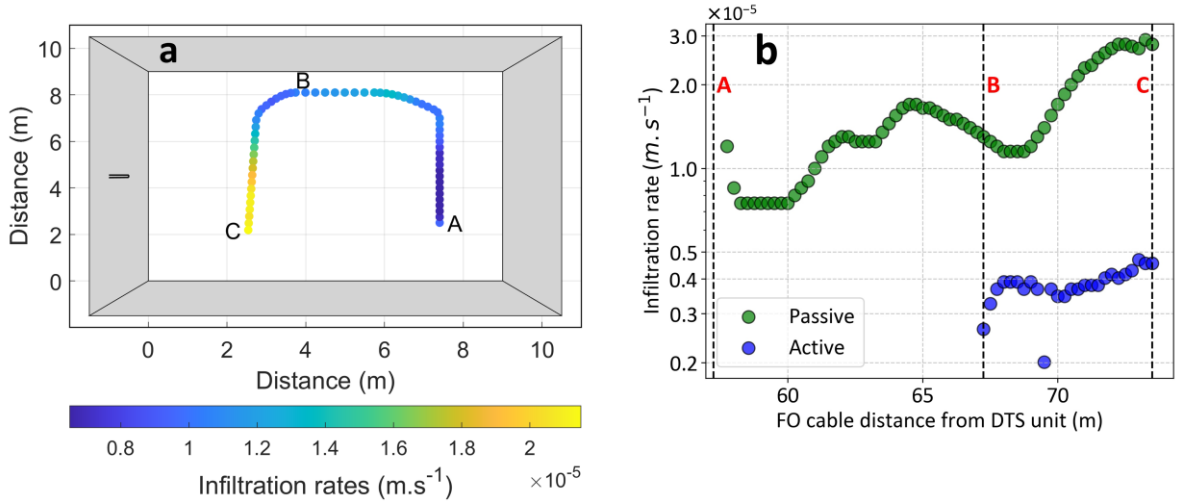

Figure 8. a) map of recharge rates derived from the interpretation of passive-DTS data; b) variation of infiltration rate along the entire buried section of the FO cable, derived from both passive and active-DTS data analysis.

3.2.3. Comparative analysis: stationary and transient infiltration rates

The pressure sensor installed within the cobblestone layer of the basin recorded water level variations during the basin-filling phase for the first seven hours and throughout the basin-emptying phase, which lasted from approximately 7 to 135 hours (Figure 9a). As the basin water level decreased over time, this decline reflected the volume of water infiltrating per unit area. The temporal derivative of the water level signal provides an estimate of the infiltration rate at the basin scale (Figure 9b). Note that the infiltration rate was not calculated during the basin-filling stage as water infiltrates simultaneously with the rising water level.

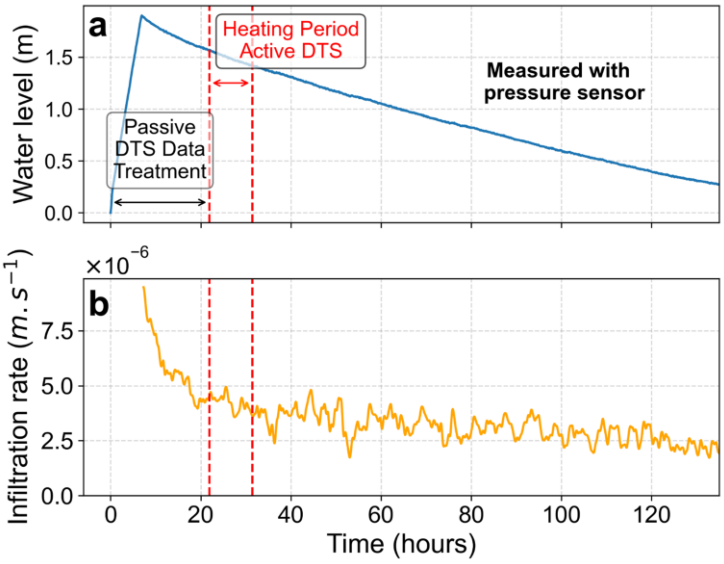

Figure 9. Pressure sensor data showing: a) water level evolution during the infiltration test, and b) the corresponding instantaneous infiltration rate derived from the temporal derivative of the water level.

Given the rapid and significant decrease in infiltration rate at the start of the test, the stationary flow conditions assumed in the numerical model for interpreting passive-DTS measurements may be inaccurate. Therefore, new simulations were conducted considering transient infiltration rates to account for the actual dynamics of the infiltration rates. The analysis focuses on a single point along the FO cable, located 70 meters from the DTS unit.

Figure 10a presents the optimized transient infiltration rate model, while Figure 10b compares the thermal response curves derived from passive-DTS data interpretation under both stationary and transient infiltration conditions. Under the assumption of stationary flow, the optimal infiltration rate was determined to be 1.35×10^{-5} m.s^{-1}. The thermal response model simulated considering transient infiltration dynamics closely aligns with the thermal response obtained under stationary conditions.

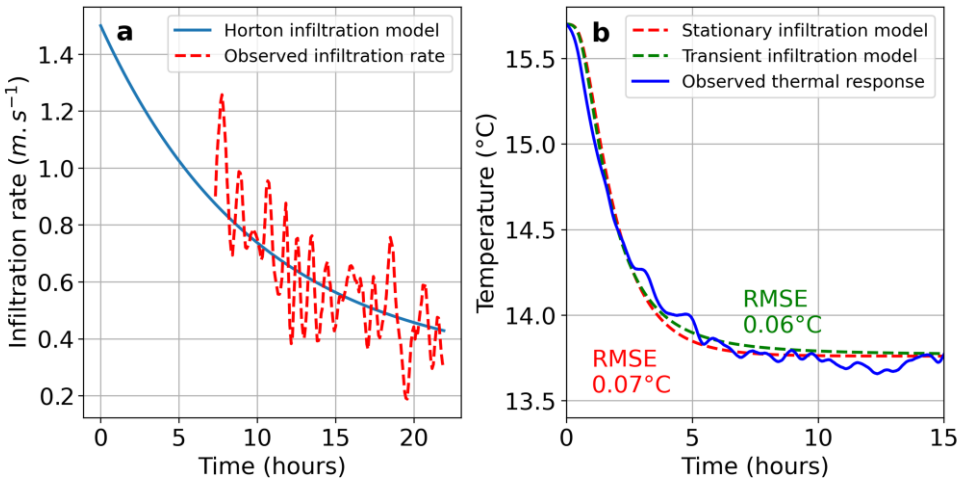

Figure 10. a) Optimized transient infiltration model with an initial infiltration rate of 1.50×10^{-5} m.s^{-1}, and b) corresponding simulated thermal response model (green dotted line) compared to the best-fit thermal model assuming a stationary infiltration rate of 1.35×10^{-5} m.s^{-1} (red dotted line).

4. Discussion

The discussion provides an in-depth examination of the findings and implications from both passive- and active-DTS data analysis. Firstly, the sensitivity of infiltration rate estimates to changes in model parameters has been evaluated. The discrepancy in results between passive- and active-DTS data interpretation is then explained by describing the differing infiltration dynamics observed during the test. The discussion also explores the spatial variability in the estimated infiltration rates, highlighting potential factors influencing these variations. Finally, the outcomes of this study with regard to MAR operations and monitoring strategies are discussed.

4.1. Sensitivity analysis on infiltration rate estimates from DTS data analysis

The interpretation of both passive- and active-DTS data relies on assumptions that may influence the reliability of the estimates. In the analysis of active-DTS data, the ADTS toolbox addresses instrumental uncertainty by assessing the impact of temperature noise on the determination of thermal conductivity and flux values. In this study, a mean temperature noise of 1 °C resulted in uncertainties of 0.28 $W \cdot m^{-1} \cdot K^{-1}$ for thermal conductivity and 2.98×10^{-6} $m \cdot s^{-1}$ for the derived infiltration rates.

The accuracy of infiltration rate estimates in passive-DTS analysis depends on the reliability of the parameters incorporated within the heat transfer numerical model. Key parameters influencing heat transfer dynamics include total porosity, volumetric heat capacity, and thermal conductivity of the saturated porous medium. Additionally, the burial depth of the FO cable introduces further uncertainty. As outlined in Section 2.5, the sensitivity assessment methodology involves computing the relative deviation of infiltration rates necessary to align with the reference model. The resulting deviations, presented in Table 2, provide insights into how variations in these parameters affect the estimated infiltration rates.

During the installation of the FO cable, efforts were made to bury it as close as possible to a depth of 10 cm. However, actual burial depth may vary slightly across different locations. To assess the impact of burial depth on thermal responses, temperature variations were modeled at depths ranging from 5 cm to 15 cm (see Figure 11a). Thermal responses simulated at shallower depths (5 cm and 7.5 cm) require a lower infiltration rate to accurately replicate the reference model, whereas those at greater depths (12.5 cm and 15 cm) require higher infiltration rates. The range of relative deviations from the reference model is from -16 to 19% for a 5-centimeter depth uncertainty and from -30 to 33% for a 10-centimeter depth uncertainty.

Similarly, the impact of the thermal conductivity on thermal response curves was evaluated by simulating temperature variations across different ranges for λ (see Figure 11b). For loess material, a thermal conductivity range of 1.5 to 3.5 $W \cdot m^{-1} \cdot K^{-1}$ is expected (Andújar et al., 2016), resulting in relative deviations from -3 to 13%. However, this range of uncertainty can be reduced by considering thermal conductivity values inferred from active-DTS data interpretation. A refined range of 1.31 to 2.17 $W \cdot m^{-1} \cdot K^{-1}$ is obtained when accounting spatial variability and the intrinsic error (0.28 $W \cdot m^{-1} \cdot K^{-1}$) associated with active-DTS measurements. This refinement leads to relative deviations from -4 to 3%.

Although the utilization of thermal conductivity data derived from active-DTS reduces uncertainty, the error remains relatively small in both cases. This can be attributed to the thermal Peclet number, a dimensionless parameter that quantifies the ratio of heat transfer by advection to conduction (Anderson, 2005). In this study, the thermal Peclet number is greater than one, indicating that heat

transfer is dominated by advection rather than conduction during the initial stages of infiltration. For more information on Peclet number calculation, please refer to Section S6 of the supplementary materials. Consequently, the sensitivity associated to thermal conductivity is relatively low. Note that even with low-permeability materials, such as loess, advection dominates heat transfer leading to low sensitivity to thermal conductivity. In more permeable materials (e.g., sand, gravel, etc…), advection would play an even more dominant role, further reducing the impact of thermal conductivity uncertainties.

The values of total porosity and volumetric heat capacity exert minimal influence on the simulated thermal response (see Figure 11c and Figure 11d). For loess, total porosity typically ranges between 36% and 55% (Zhang *et al.*, 2023), although Delvoie (2017) refined this range to 40%–46% in their study on Hesbaye loess characterization. Within this refined interval, variations in the inferred infiltration rate remain below 1%. Even when considering more extreme porosity values, the resulting deviation does not exceed 3%. This finding indicates that the uncertainty associated with porosity has a negligible effect on infiltration rate estimates. Conversely, the volumetric heat capacity of saturated loess exerts a slightly greater influence on model outcomes. The expected values for this parameter range between 2.5 and 3.5 $MJ \cdot m^{-3} \cdot K^{-1}$ (Khaled A and Nidal H, 2020), leading to a calculated relative deviation of 9% in infiltration rate estimates.

A worst-case scenario is considered, incorporating a 5-centimeter depth uncertainty in FO cable placement, thermal conductivity values ranging from 1.31 to 2.17 $W \cdot m^{-1} \cdot K^{-1}$ (inferred from active-DTS analysis), volumetric heat capacities between 2.5 and 3.5 $MJ \cdot m^{-3} \cdot K^{-1}$, and porosity values from 36% to 55%. The maximum deviation in estimated infiltration rates is thus approximately 30%. This level of uncertainty is comparable to that associated with conventional in-situ infiltration measurement techniques, such as lysimeters and double-ring infiltrometers, which also demonstrate uncertainties up to 30% (Amaral *et al.*, 2018; Rönnqvist, 2018; Silva *et al.*, 2020). However, these methods provide only localized measurements, whereas DTS-based approaches offer spatially integrated estimations of infiltration, reducing the impact of site-specific variability. Despite these advantages, the burial depth of the FO cable remains a critical factor in minimizing uncertainty. Improving cable installation procedures could significantly reduce depth-related errors and enhance the accuracy of DTS-based measurements.

While the sensitivity analysis provides valuable insights into how variations in key parameters influence thermal response and infiltration rate estimates, extending this uncertainty quantification along the entire buried fiber optic cable is not feasible. This finding further validates the enhanced reliability of the active-DTS method in comparison to passive-DTS measurements. However, it's important to consider this perspective with nuance. Active-DTS data analysis provides highly accurate infiltration rates at any stage of the infiltration test, whereas passive-DTS data interpretation offers insights into initial infiltration rates but with higher uncertainty. Nevertheless, the passive-DTS method remains more reliable than traditional in-situ techniques because it provides spatially resolved values at the scale of a pilot site.

Table 2. Relative deviation in estimated infiltration rate due to parameter variation in COMSOL.

	depth (cm)	**q_{model} ($m \cdot s^{-1}$)**	**Relative deviation (%)**
d_1	5	7.35×10^{-6}	-30
d_2	7.5	8.85×10^{-6}	-16
d_3	12.5	1.25×10^{-5}	19
d_4	15	1.40×10^{-5}	33
	thermal conductivity ($W \cdot m^{-1} \cdot K^{-1}$)	**q_{model} ($m \cdot s^{-1}$)**	**Relative deviation (%)**
λ_1	1.31	1.01×10^{-5}	-4
λ_2	1.50	1.02×10^{-5}	-3
λ_3	2.17	1.08×10^{-5}	3
λ_4	3.50	1.19×10^{-5}	13
	Volumetric heat capacity ($MJ \cdot m^{-3} \cdot K^{-1}$)	**q_{model} ($m \cdot s^{-1}$)**	**Relative deviation (%)**
VHC_1	2.5	9.50×10^{-6}	-9
VHC_2	3.5	1.14×10^{-5}	9
	Porosity (%)	**q_{model} ($m \cdot s^{-1}$)**	**Relative deviation (%)**
n_1	36	1.06×10^{-5}	1
n_2	40	1.05×10^{-5}	0
n_3	46	1.04×10^{-5}	-1
n_4	55	1.02×10^{-5}	-3

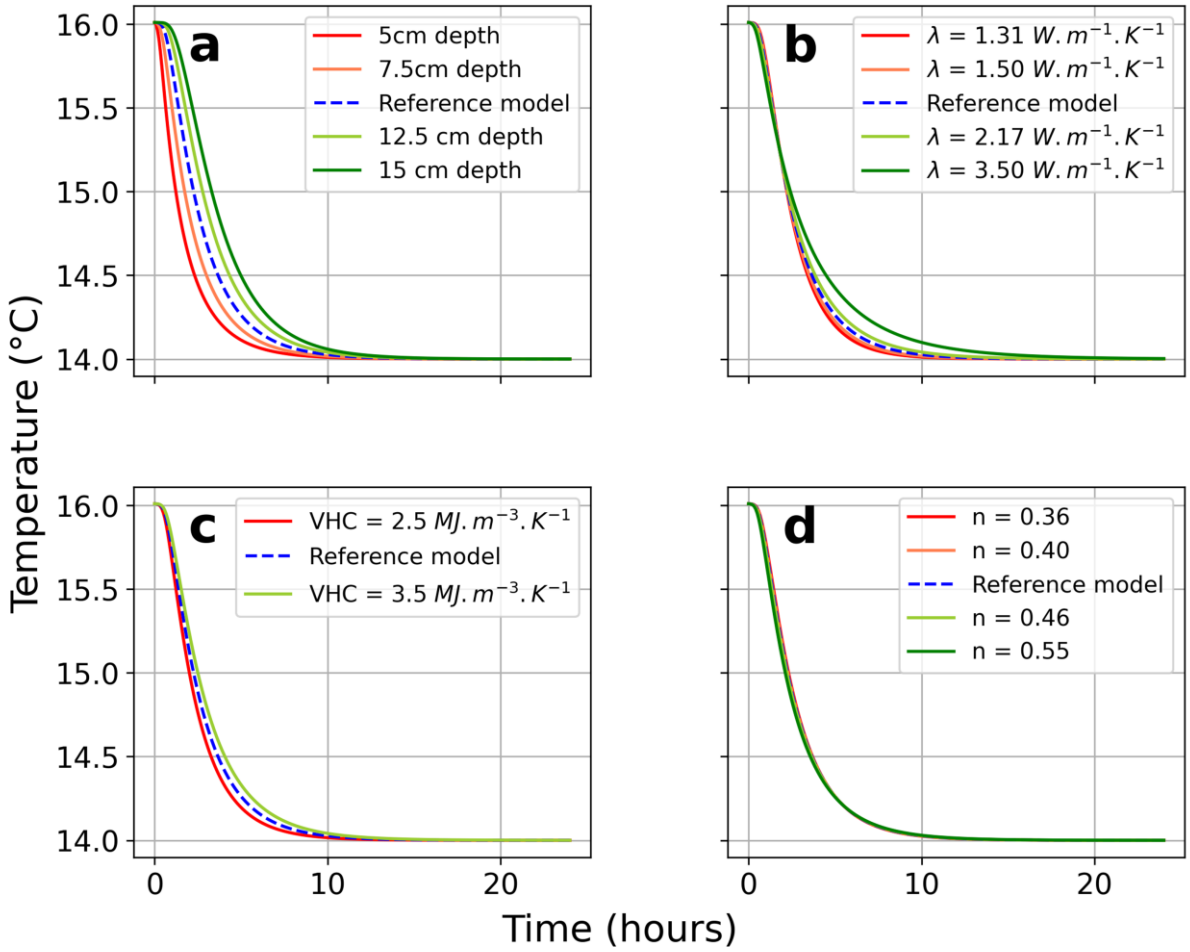

Figure 11. Sensitivity of thermal response models to variations in a) depth, b) thermal conductivity, c) volumetric heat capacity (VHC) and d) total porosity.

4.2. Temporal variations in infiltration rates

Estimates of infiltration rates derived from active- and passive-DTS measurements differ by one order of magnitude. Passive-DTS data interpretation yielded a higher mean recharge rate of 1.51×10^{-5} m·s^{-1}, compared to 3.79×10^{-6} m·s^{-1} from active-DTS data analysis. As outlined in Section 4.1, the impact of parameter uncertainty on these estimates is minimal, with a maximum reasonable deviation of approximately 30%. This finding suggests that the observed discrepancy in magnitude between passive and active-DTS interpretations cannot be attributed to parameter uncertainty, but rather to the temporal dynamics of infiltration (see Figure 9b).

To further validate this interpretation, infiltration rates derived from DTS analysis were compared with those inferred from pressure data. Passive-DTS measurements reflect infiltration rates during the early stage of the infiltration test, whereas active-DTS measurements were conducted 24 hours later. The higher infiltration rates estimated from passive-DTS represent the initial rapid infiltration before decreasing exponentially over time, as described in Horton's theory (1933, 1939). These findings are consistent with the behavior observed from pressure data (see Figure 9b). Given that the infiltration rate measured from pressure data is representative of basin-scale infiltration, the mean infiltration rate derived from active-DTS, which integrates variations along the FO cable, provides a suitable basis for comparison. In fact, the mean infiltration rate obtained from pressure data during the heating

period was approximately 4×10^{-6} m·s^{-1}, which aligns well with the 3.79×10^{-6} m·s^{-1} derived from active-DTS. These values are consistent with those reported in studies of infiltration basins with loamy sediments (Beganskas and Fisher, 2017), supporting the validity of the applied approach. It is important to note that the actively heated segment of the FO cable traverses only the left portion of the infiltration basin (see Figure 6a). Therefore, the mean infiltration rate obtained from active-DTS analysis may not fully represent the recharge dynamics across the entire basin. This consideration underscores the importance of incorporating the temporal dynamics of infiltration, a component frequently overlooked in conventional methods that prioritize the initial stages of infiltration, such as lysimeters.

On July 25th 2023, groundwater levels were measured in two piezometers located a few meters from the infiltration basin. These measurements indicate that the basin and the aquifer are unlikely to be hydraulically connected. This suggests that the temporal evolution of infiltration is governed by processes within the unsaturated zone, rather than by direct hydraulic interaction with the aquifer. As infiltration progresses, a dynamic water front delineates the saturated and unsaturated zones within the soil (Alastal and Ababou, 2019), with pressure data revealing a gradual decline in the recharge rate, from approximately 4×10^{-6} m·s^{-1} to 2×10^{-6} m·s^{-1}, before the water level reaches the top of the pebblestone layer. According to Darcy's law, the reduction in infiltration rate can be attributed to the diminishing pressure head, which results in decreased groundwater flux and, consequently, a lower recharge rate. This phenomenon has been notably documented by Helles and Mogheir (2022), who observed a linear decrease in infiltration rates in permeable stormwater basins as the pond water depth decreased.

Given that passive-DTS interpretation assumes steady-state flow, we assessed the potential influence of transient conditions through additional simulations. The infiltration rate derived from passive-DTS data at a distance of 70 meters from the DTS unit (see Section 3.2.2), estimated at 1.35×10^{-5} m·s^{-1}, is slightly lower than the initial rate of 1.50×10^{-5} m·s^{-1} used in the transient recharge model (see Section 3.2.3). This slight underestimation suggests that, while passive-DTS interpretation provides valuable insights into early infiltration dynamics, it may not fully capture the rapid changes occurring during the initial phase of infiltration. However, the difference (approximately 10%) is relatively small compared to the inherent variability of infiltration rates. Nevertheless, it is important to acknowledge that this difference (1.5×10^{-6} m·s^{-1}) is smaller than the uncertainty associated with the estimates evaluated in the sensitivity analysis. Consequently, this underestimation may also be a result of the inherent uncertainty in the measurements and analysis, rather than indicative of a systematic error in the passive-DTS interpretation approach.

While the transient recharge model offers valuable insights into infiltration dynamics, its application along the entire FO cable presented certain limitations. At points where temperature changes were slower, it was difficult to assign a sufficiently low initial infiltration rate that matched the observed data. This challenge arises because the infiltration data inferred from water pressure measurements reflect average values across the system and cannot account for localized deviations in soil properties. While the transient recharge model provides a more comprehensive representation of the infiltration process dynamics, the approximation using a constant infiltration rate for passive-DTS data analysis is adequate for estimating the spatial distribution of recharge rates at the onset of the infiltration test. Therefore, The necessity of considering transient recharge at every point along the FO cable for passive-DTS data interpretation may not be necessary for practical applications. The constant

infiltration rate approximation offers an efficient and effective approach for assessing initial infiltration rates over space, without significantly altering the overall interpretation. However, it is important to note that this conclusion is specific to the present study site and that differing soil conditions at other sites may yield different results.

In light of these findings, future work should focus on developing methods to integrate transient infiltration models that reproduce thermal responses from passive-DTS data, thereby capturing the temporal dynamics of early recharge rather than assuming constant infiltration rates. Such models would enable a more accurate representation of the evolving infiltration process. While most DTS-based studies rely on longer time series (e.g., days to months) and focus on broader-scale patterns such as diurnal variations (Hatch *et al.*, 2006), few have addressed infiltration dynamics at the short time scales (seconds to minutes) that characterize early recharge. The high temporal resolution of the measurements (10 s) enables a more detailed capture of infiltration rate changes, underscoring the need to develop new methodologies for transient recharge model integration in such contexts.

4.3. Spatial distribution of infiltration rates

As illustrated in Figure 6a and Figure 8a, infiltration rates exhibit spatial variability, with a slight increase observed along the heated section of the FO cable (from B to C). The consistency of this trend across both passive- and active-DTS data interpretations (Figure 8b) reinforces the reliability of the results. Several factors may explain these observed differences. As indicated in the sensitivity analysis, the depth at which the fiber is buried affects the inferred infiltration rates. Therefore, a gradual increase in burial depth from point B to point C could partly explain the rising infiltration estimates along the heated section. Additionally, slight irregularities in the sediment surface, such as a subtle slope, may cause small variations in water depth, contributing to differences in the results. It is likely that a combination of these factors accounts for the observed variability. Nevertheless, the variations remain relatively minor, and the method proves effective for identifying meaningful spatial differences.

Furthermore, the interpretation of passive-DTS data reveals lower fluxes along the B-A section compared to B-C. In addition to the effects of burial depth and sloped sediment surface, a plausible explanation is that the B-C section lies directly beneath the basin's filling pipe. Since passive-DTS data capture conditions at the onset of the infiltration test, turbulence from the incoming water may locally enhance infiltration by temporarily increasing pressure and scouring fine sediments (Maltauro *et al.*, 2024). This process could lead to higher initial infiltration rates on that side of the basin.

These observations raise the question of whether the spatial patterns reflect actual variability or measurement uncertainty. As indicated in the sensitivity analysis, variations in burial depth can cause the estimated infiltration rate at a single point to range from 7.35×10^{-6} to 1.4×10^{-5} $m \cdot s^{-1}$. Conversely, the interpretation of passive-DTS data reveals a spatial variability from 7.5×10^{-6} to 1.7×10^{-5} $m \cdot s^{-1}$, falling within the same range. This suggests that the apparent spatial differences may reflect methodological uncertainty rather than actual heterogeneity in soil properties. This represents a significant limitation of the passive-DTS method, as the uncertainty associated with burial depth is of the same order of magnitude as the spatial variability it aims to capture. Nevertheless, the spatial trend in infiltration rates derived from passive-DTS measurements is consistent with that observed in active-DTS measurements (Figure 8b). This agreement reinforces the reliability of the observed increase in groundwater flux from B to C, despite the underlying uncertainties. It also underscores the value of

conducting active-DTS measurements in parallel with passive-DTS to accurately capture spatial variability.

4.4. Strengths and Limitations of Passive and Active-DTS Methods

Both active and passive-DTS approaches offer distinct advantages and limitations. Active-DTS provides accurate infiltration rate estimates with high spatial resolution and low associated uncertainty. In contrast to passive-DTS, it does not rely on natural temperature variations, enabling estimation of recharge rates at any time during the infiltration process. Moreover, active-DTS can be applied year-round, regardless of the temperature contrast between the soil and the recharge water. However, this method requires the injection of electric current into the steel armoring of the FO cable to generate heat, making it reliant on an external power supply. As a result, active-DTS may not be optimal for long cable sections (e.g., over several hundred meters), where uniform heating would require substantially higher power.

In contrast, passive-DTS interpretation provides estimates of the initial infiltration rate, primarily capturing the early and more rapid phase of infiltration. Nevertheless, passive-DTS measurements offer the advantage of covering a larger spatial domain, as DTS units are capable of monitoring temperature variations across several hundred meters. However, as discussed in Section 4.1, the numerical model used to interpret passive-DTS data is subject to input-related uncertainties. In particular, uncertainty in the burial depth of the FO cable introduces a 19% to 33% margin of error in recharge estimates, which complicates the detection of small flux variations.

Conversely, active-DTS remains largely unaffected by burial depth. Only two specific conditions regarding burial depth could influence active-DTS measurements. First, as demonstrated by Simon *et al.* (2024), if the cable is buried less than 3 cm, a portion of the generated heat may dissipate to the surface, thereby reducing the measured temperature increase. Secondly, filtering out natural temperature fluctuations in active-DTS data typically requires support from passive-DTS measurements. Therefore, it is essential to apply an appropriate filtering procedure. In this study, the cable was buried deep enough to avoid interference from surface heat exchange. Passive-DTS data were filtered accordingly before interpreting active-DTS results (see Section 2.3.1). Therefore, active-DTS measurements can be considered effectively independent of the cable's burial depth in this context.

The reliability of passive-DTS data, on the other hand, depends on achieving a sufficient temperature contrast between the infiltrating water and the surrounding soil. This contrast must exceed both the instrument's noise level and any natural temperature fluctuations occurring during basin replenishment. In this study, conducted in July, the temperature difference was approximately 2°C, well above the DTS noise level of 0.05°C. Based on the mean stabilized temperature recorded along the FO cable and its associated noise, we calculated a mean signal-to-noise ratio (SNR) of 49 dB, indicating a high-quality signal (Young, 2015). Maintaining infiltration rate estimates within a 10% error margin requires a minimum temperature difference of 1 °C when noise is 0.05 °C (i.e., $\Delta T > 20 \times$ noise). Conducting studies in colder seasons or climates may benefit from larger contrasts between soil and infiltrating water. Alternatively, temperature contrast limitations can be addressed through the analysis of natural temperature signal propagation at various depths, as demonstrated by Becker *et al.* (2013) and Mawer *et al.* (2016). Their method uses phase shifts in diurnal temperature signals detected by co-located FO cables at various depths to estimate infiltration rates. This approach enables the

inference of daily infiltration dynamics and their spatial variability. However, it requires cables to be installed at multiple depths, which presents technical challenges.

Overall, combining both active and passive-DTS data is particularly advantageous. Passive-DTS provides estimates of the initial infiltration rate over a broad spatial extent. Conversely, active-DTS provides accurate estimates during the infiltration period. Furthermore, as emphasized by Simon *et al. (2022)*, estimating the thermal conductivity of sediments with active-DTS data significantly reduces uncertainties in passive-DTS-derived infiltration rates. Without these estimates, the model would rely on a broader range of thermal conductivity values from the literature, thereby increasing the uncertainty of the results.

4.5. Use of DTS technology in MAR schemes

DTS-based methods have proven highly effective for estimating recharge rates and offer significant advantages for MAR operation management. Their ability to provide high-resolution spatial data enhances understanding of hydrological dynamics within infiltration basins. By burying a FO cable in the basin sediments, it becomes possible to monitor the spatial distribution of recharge and detect preferential infiltration pathways, leading to multiple operational benefits.

A key application of this capability is the detection and management of clogging, a common issue in MAR systems that leads to reduced infiltration efficiency due to the formation of low-permeability layers beneath the basin (Van Cuyk, 2001; Pavelic *et al.*, 2011; Barry *et al.*, 2017). As demonstrated by Medina *et al.* (2020), repeated DTS surveys can effectively identify zones of reduced infiltration caused by clogging. This information enables targeted maintenance, helping to minimize downtime and preserve system performance. Beyond maintenance, DTS also supports real-time optimization of water delivery. By adjusting ponding depth and flow rates in response to spatially resolved temperature data, operators can enhance infiltration efficiency and adapt to changing conditions. This contributes to more sustainable and cost-effective MAR operations.

Integrating DTS data into operational decision-making allows for more precise control over recharge processes, ultimately improving groundwater management. Future research should explore long-term monitoring to assess the effectiveness of various operational strategies, such as maintaining steady water levels or alternating between wetting and drying cycles. Additionally, exploring the integration of DTS with other monitoring technologies could further enhance MAR management by improving diagnostic capabilities and ensuring the long-term reliability and effectiveness of these critical systems.

5. Conclusion

Passive- and active-DTS measurements were conducted during an infiltration test to demonstrate the applicability of the technology to accurately quantify recharge rates within the framework of MAR. The results demonstrate that DTS methods are particularly well suited for capturing the spatial variability of infiltration rates, an important advantage given the challenges associated with estimating soil hydraulic permeability. In this study, DTS provided direct and reliable estimates of infiltration, offering valuable insight into the soil's infiltration capacity and enhancing the overall understanding of recharge dynamics.

DTS measurements were carried out along a FO cable, buried within the loess sediments forming the base of the infiltration basin. These fine-grained materials, which are typically characterized by low to moderate permeability, are often overlooked in MAR applications. However, the infiltration rates

inferred from DTS measurements in this study were found to be relatively high, ranging between 33 and 130 cm·day^{-1}. These findings suggest that loess-based systems can support effective infiltration under the specific environmental conditions observed at the study site. Conducting similar studies in comparable geological contexts would underscore the importance of not systematically excluding loess sediments when assessing the feasibility of MAR. Moreover, the observed infiltration rates are comparable to those reported for sandy materials in Soil Aquifer Treatment (SAT), such as those documented in Negev *et al.* (2020), where rates ranged from 48 to 120 cm·day^{-1}. This comparison underscores the potential of loess to support recharge capacities similar to those of more permeable materials when managed appropriately. As such, the results indicate that MAR can be successfully implemented in regions where high-permeability soils are limited, contributing to the long-term sustainability of groundwater recharge strategies across diverse environments. By demonstrating the viability of loess for effective infiltration, this study opens new perspectives for MAR implementation in areas traditionally deemed unsuitable.

Beyond the clear advantage of using DTS technology to quantify spatial variations in infiltration rates, the combined application of active- and passive-DTS measurements also offers valuable insights into the temporal dynamics of infiltration. Passive-DTS measurements were analyzed during the early phase of the test to capture natural temperature changes in the soil induced by infiltrating water. In contrast, active-DTS measurements are independent of natural temperature fluctuations and can be conducted anytime during the infiltration process. This flexibility offers a significant advantage, as repeated active-DTS surveys enable continuous monitoring of infiltration dynamics over time, enhancing the understanding and managed of MAR system performance.

Future research should prioritize long-term monitoring to evaluate the effectiveness of various operational strategies. In particular, comparative studies between constant water level infiltration and alternating wetting-drying cycles could help determine the most efficient approach for optimizing MAR system performance.

Data availability

The data presented in the paper are available and accessible through the following link in the ULiège dataverse: https://doi.org/10.58119/ULG/SZTN6A.

Acknowledgements

This experimentation was made possible through collaboration with the regional water distribution company, CILE (Compagnie Intercommunale Liégeoise des Eaux), which granted access to their installation facility and provided clean abstracted groundwater to fill the infiltration basin.

The characterization of loess properties was carried out at the Building Materials Laboratory (LMC) within the Urban and Environmental Engineering (UEE) department at the University of Liège, under the supervision of Pierre Illing. We are sincerely grateful to him for his valuable assistance in conducting the measurements of the physico-thermal properties of the loess sediments.

Funding

Robin Glaude is a beneficiary of the ASP-REN fellowship supported by the FNRS (Fonds de la Recherche Scientifique) Belgium. Nataline Simon is a beneficiary of the IPD-STEAM fellowship supported by the Special Funds for Research.

Part of the DTS equipment was acquired with the support of the FNRS Belgium (grant No. J.0023.22).

References

[1] Alastal, K. and Ababou, R., 2019. Moving Multi-Front (MMF): A generalized Green-Ampt approach for vertical unsaturated flows. Journal of Hydrology. 579, p. 124184. https://doi.org/10.1016/j.jhydrol.2019.124184.

[2] Amaral, A. M., Cabral Filho, F. R., Vellame, L. M., Teixeira, M. B., Soares, F. A. and dos Santos, L. N., 2018. Uncertainty of weight measuring systems applied to weighing lysimeters. Computers and Electronics in Agriculture, 145, 208-216. https://doi.org/10.1016/j.compag.2017.12.033.

[3] Amy, G. and Drewes, J., 2007. Soil Aquifer Treatment (SAT) as a Natural and Sustainable Wastewater Reclamation/Reuse Technology: Fate of Wastewater Effluent Organic Matter (EfOM) and Trace Organic Compounds. Environmental Monitoring and Assessment. 129(1–3), pp. 19–26. https://doi.org/10.1007/s10661-006-9421-4.

[4] Anderson, M.P., 2005. Heat as a Ground Water Tracer. Groundwater. 43(6), pp. 951–968. https://doi.org/10.1111/j.1745-6584.2005.00052.x.

[5] Andújar Márquez, J., Martínez Bohórquez, M. and Gómez Melgar, S., 2016. Ground Thermal Diffusivity Calculation by Direct Soil Temperature Measurement. Application to very Low Enthalpy Geothermal Energy Systems. Sensors. 16(3), p. 306. https://doi.org/10.3390/s16030306.

[6] Barry, K., Vanderzalm, J., Miotlinski, K. and Dillon, P., 2017. Assessing the Impact of Recycled Water Quality and Clogging on Infiltration Rates at A Pioneering Soil Aquifer Treatment (SAT) Site in Alice Springs, Northern Territory (NT), Australia. Water. 9(3), p. 179. https://doi.org/10.3390/w9030179.

[7] Batlle Aguilar, J., Orban, P., Dassargues, A. and Brouyère, S., 2007. Identification of groundwater quality trends in a chalk aquifer threatened by intensive agriculture in Belgium. Hydrogeology Journal. 15(8), pp. 1615–1627. https://doi.org/10.1007/s10040-007-0204-y.

[8] Becker, M.W., Bauer, B. and Hutchinson, A., 2013. Measuring Artificial Recharge with Fiber Optic Distributed Temperature Sensing. Groundwater. 51(5), pp. 670–678. https://doi.org/10.1111/j.1745-6584.2012.01006.x.

[9] Beganskas, S. and Fisher, A.T., 2017. Coupling distributed stormwater collection and managed aquifer recharge: Field application and implications. Journal of Environmental Management. 200, pp. 366–379. https://doi.org/10.1016/j.jenvman.2017.05.058.

[10] Bense, V.F., Read, T., Bour, O., Le Borgne, T., Coleman, T., Krause, S., Chalari, A., Mondanos, M., Ciocca, F. and Selker, J. S., 2016. Distributed Temperature Sensing as a downhole tool in hydrogeology. Water Resources Research. 52(12), pp. 9259–9273. https://doi.org/10.1002/2016WR018869.

[11] Bilskie, J.R., 1994. Dual probe methods for determining soil thermal properties: numerical and laboratory study. Doctor of Philosophy. Iowa State University, Digital Repository. https://doi.org/10.31274/rtd-180813-11719.

[12] Bonilla Valverde, J.P., Blank, C., Roidt, M., Schneider, L. and Stefan, C., 2016. Application of a GIS Multi-Criteria Decision Analysis for the Identification of Intrinsic Suitable Sites in Costa Rica for the Application of Managed Aquifer Recharge (MAR) through Spreading Methods. Water. 8(9), p. 391. https://doi.org/10.3390/w8090391.

[13] Boretti, A. and Rosa, L., 2019. Reassessing the projections of the world water development report. NPJ Clean Water, 2(1), 15.

[14] Bouwer, H., 1986. Intake Rate: Cylinder Infiltrometer. In: Klute, A., Ed., Methods of Soil Analysis, ASA Monograph 9, ASA, Madison, pp. 825–844.

[15] Bouwer, H., 2002. Artificial recharge of groundwater: hydrogeology and engineering. Hydrogeology Journal. 10(1), pp. 121–142. https://doi.org/10.1007/s10040-001-0182-4.

[16] Bouwer, H., Pyne, R. D. G. and Brown, J., 2008. Design, Operation, and Maintenance for Sustainable Underground Storage Facilities. In American Water Works Association Research Foundation Report; AWWA Research Foundation and IWA: Denver, CO, USA.

[17] Brouyère, S., 2001. Etude et Modélisation du Transport et du Piégeage des Solutés en Milieu Souterrain Variablement Saturé. University of Liège, Liège, Belgium.

[18] Caligaris, E., Agostini, M. and Rossetto, R. , 2022. Using Heat as a Tracer to Detect the Development of the Recharge Bulb in Managed Aquifer Recharge Schemes. Hydrology. 9(1), p. 14. https://doi.org/10.3390/hydrology9010014.

[19] Calvin, K. et al., 2023. IPCC, 2023: Climate Change 2023: Synthesis Report. Contribution of Working Groups I, II and III to the Sixth Assessment Report of the Intergovernmental Panel on Climate Change [Core Writing Team, H. Lee and J. Romero (eds.)]. IPCC, Geneva, Switzerland.

[20] CILE, 2022. CILE: rapport annuel 2022. https://www.cile.be/sites/default/files/2023-07/CILE%20rapport%20annuel%202022.pdf (Accessed 23 October 2024).

[21] COMSOL (2023). *COMSOL Multiphysics® v. 6.3*. COMSOL AB, Stockholm, Sweden. https://www.comsol.com .

[22] Constantz, J., 2008. Heat as a tracer to determine streambed water exchanges. Water Resources Research. 44(4). https://doi.org/10.1029/2008WR006996.

[23] Del Val, L., Carrera, J., Pool, M., Martínez, L., Casanovas, C., Bour, O. and Folch, A., 2021. Heat Dissipation Test With Fiber-Optic Distributed Temperature Sensing to Estimate Groundwater Flux. Water Resources Research. 57(3), p. e2020WR027228. https://doi.org/10.1029/2020WR027228.

[24] Delvoie, S. (2017) Caractérisation multiéchelle du lœss de Hesbaye (Belgique) par une approche couplée géologique et géotechnique. Liège University

[25] Des Tombe, B.F., Mark, B, Smits, F., Schaars, F. and Van Der Made, K-J., 2019. Estimation of the Variation in Specific Discharge Over Large Depth Using Distributed Temperature Sensing (DTS) Measurements of the Heat Pulse Response. Water Resources Research. 55(1), pp. 811–826. https://doi.org/10.1029/2018WR024171.

[26] Dillon, P., 2005. Future management of aquifer recharge. Hydrogeology Journal. 13(1), pp. 313–316. https://doi.org/10.1007/s10040-004-0413-6.

[27] Dillon, P., 2009. Managed aquifer recharge: an introduction. Waterlines Report Series, National Water Commission, Canberra.

[28] Gilmore, T. E., Johnson, M., Korus, J., Mittelstet, A., Briggs, M. A., Zlotnik, V., and Corcoran, S., 2019. Streambed Flux Measurement Informed by Distributed Temperature Sensing Leads to a Significantly Different Characterization of Groundwater Discharge. Water. 11(11), p. 2312. https://doi.org/10.3390/w11112312.

[29] Goderniaux, P., Orban, P., Rorive, A., Brouyère, S., and Dassargues, A., 2023. Study of historical groundwater level changes in two Belgian chalk aquifers in the context of climate change impacts. Geological Society, London, Special Publications. 517(1), pp. 203–211. https://doi.org/10.1144/SP517-2020-212.

[30] Green, T. R., Taniguchi, M., Kooi, H., Gurdak, J. J., Allen, D. M., Hiscock, K. M., Treidel, H., Aureli, A., 2011. Beneath the surface of global change: Impacts of climate change on groundwater. Journal of Hydrology. 405(3–4), pp. 532–560.https://doi.org/10.1016/j.jhydrol.2011.05.002.

[31] Hakoun, V., Orban, P., Dassargues, A. and Brouyère, S., 2017. Factors controlling spatial and temporal patterns of multiple pesticide compounds in groundwater (Hesbaye chalk aquifer, Belgium). Environmental Pollution. 223, pp. 185–199. https://doi.org/10.1016/j.envpol.2017.01.012.

[32] Hatch, C.E., Fisher, A.T., Revenaugh, J.S., Constantz, J. and Ruehl, C., 2006. Quantifying surface water-groundwater interactions using time series analysis of streambed thermal records: Method development: TIME SERIES THERMAL METHOD QUANTIFIES SW-GW. Water Resources Research, 42(10). https://doi.org/10.1029/2005WR004787.

[33] Hausner, M. B., Suárez, F., Glander, K. E., Giesen, N. v. d., Selker, J. S., and Tyler, S. W., 2011. Calibrating Single-Ended Fiber-Optic Raman Spectra Distributed Temperature Sensing Data. Sensors. 11(11), pp. 10859–10879. https://doi.org/10.3390/s111110859.

[34] Helles, Z. and Mogheir, Y., 2022. Factors Affecting the Infiltration Rate of Stormwater. TIJER Technix International Journal for Engineering Research. 9(8), pp. 72-85.

[35] Horton, R., 1933. The Rôle of infiltration in the hydrologic cycle. Eos, Transactions American Geophysical Union. 14(1), pp. 446–460. https://doi.org/10.1029/TR014i001p00446.

[36] Horton, R., 1939. Analysis of runoff-plat experiments with varying infiltration-capacity. Eos, Transactions American Geophysical Union. 20(4), pp. 693–711. https://doi.org/10.1029/TR020i004p00693.

[37] Kallali, H., Anane, M., Jellali, S. and Tarhouni, J., 2007. GIS-based multi-criteria analysis for potential wastewater aquifer recharge sites. Desalination. 215(1–3), pp. 111–119. https://doi.org/10.1016/j.desal.2006.11.016.

[38] Alnefaie, K. A. and Abu-Hamdeh, N. H., 2013. Specific heat and volumetric heat capacity of some saudian soils as affected by moisture and density. In International conference on mechanics, fluids, heat, elasticity and electromagnetic fields, pp. 139-143.

[39] Koruk, K., Yilmaz, K. K., Akyurek, Z. and Binley, A., 2020. A multi-technique approach to determine temporal and spatial variability of groundwater-stream water exchange. Hydrological Processes. 34(11), pp. 2612–2627. https://doi.org/10.1002/hyp.13754.

[40] Kurylyk, B. L., Irvine, D. J., Carey, S. K., Briggs, M. A., Werkema, D. D. and Bonham, M., 2017. Heat as a groundwater tracer in shallow and deep heterogeneous media: Analytical solution, spreadsheet tool, and field applications. Hydrological processes, 31(14), 2648-2661. https://doi.org/10.1002/hyp.11216.

[41] Le Lay, H., Thomas, Z., Rouault, F., Pichelin, P., and Moatar, F., 2019. Characterization of Diffuse Groundwater Inflows into Streamwater (Part I: Spatial and Temporal Mapping Framework Based on Fiber Optic Distributed Temperature Sensing). Water. 11(11), p. 2389. https://doi.org/10.3390/w11112389.

[42] Maliva, R.G., 2015. Managed aquifer recharge: state-of-the-art and opportunities. Water Supply. 15(3), pp. 578–588. https://doi.org/10.2166/ws.2015.009.

[43] Maltauro, R., Stone, M., Collins, A. L. and Krishnappan, B. G., 2024. Advancing mechanistic understanding of cohesive sediment transport: Integrating flume experiments, field measurements, and modelling approaches in a gravel-bed river. Science of the Total Environment, 956, 177301. https://doi.org/10.1016/j.scitotenv.2024.177301.

[44] Mawer, C., Parsekian, A., Pidlisecky, A. and Knight, R., 2016. Characterizing Heterogeneity in Infiltration Rates During Managed Aquifer Recharge. Groundwater. 54(6), pp. 818–829. https://doi.org/10.1111/gwat.12423.

[45] Medina, R., Pham, C., Plumlee, M. H., Hutchinson, A., Becker, M. W. and O'Connell, P. J., 2020. Distributed temperature sensing to measure infiltration rates across a groundwater recharge basin. Groundwater, 58(6), 913-923. https://doi.org/10.1111/gwat.13007.

[46] Nadav, I., Arye, G., Tarchitzky, J and Chen, Y., 2012. Enhanced infiltration regime for treated-wastewater purification in soil aquifer treatment (SAT). Journal of Hydrology. 420–421, pp. 275–283. https://doi.org/10.1016/j.jhydrol.2011.12.013.

[47] Orban, P., Brouyère, S., Compère, J-M., Six, S., Goderniaux, P. and Dassargues, A., 2014. Aquifère crayeux de Hesbaye. In A. Dassargues and K. Walraevens, Watervoerende lagen en grondwater in België / Aquiferes et eaux souterraines en Belgique, Academia Press, Gent, Belgium.

[48] Orban, P., Brouyère, S., Compère, J-M., Six, S., Goderniaux, P. and Dassargues, A., 2014. Aquifère crayeux de Hesbaye. In A. Dassargues and K. Walraevens, Watervoerende lagen en grondwater in België / Aquiferes et eaux souterraines en Belgique, Academia Press, Gent, Belgium.

[49] Page, D., Bekele, E., Vanderzalm, J., & Sidhu, J., 2018. Managed Aquifer Recharge (MAR) in Sustainable Urban Water Management. Water. 10(3), p. 239. https://doi.org/10.3390/w10030239.

[50] Pavelic, P., Dillon, P. J., Mucha, M., Nakai, T., Barry, K. E., Bestland, E., 2011. Laboratory assessment of factors affecting soil clogging of soil aquifer treatment systems. Water Research. 45(10), pp. 3153–3163. https://doi.org/10.1016/j.watres.2011.03.027.

[51] Pidlisecky, A. and Knight, R., 2011. The Use of Wavelet Analysis to Derive Infiltration Rates from Time-Lapse One-Dimensional Resistivity Records. Vadose Zone Journal. 10(2), pp. 697–705. https://doi.org/10.2136/vzj2010.0049.

[52] Prathapar, S., Dhar, S., Rao, G. T. and Maheshwari, B., 2015. Performance and impacts of managed aquifer recharge interventions for agricultural water security: A framework for evaluation. Agricultural Water Management. 159, pp. 165–175. https://doi.org/10.1016/j.agwat.2015.06.009.

[53] Racz, A.J., Fisher, A. T., Schmidt, C. M., Lockwood, B. S. and Huertos, M. L, 2012. Spatial and Temporal Infiltration Dynamics During Managed Aquifer Recharge. Groundwater. 50(4), pp. 562–570. https://doi.org/10.1111/j.1745-6584.2011.00875.x.

[54] Read, T., Bour, O., Selker, J. S., Bense, V. F., Le Borgne, T., Hochreutener, R. and Lavenant, N., 2014. Active-distributed temperature sensing to continuously quantify vertical flow in boreholes. Water Resources Research. 50(5), pp. 3706–3713. https://doi.org/10.1002/2014WR015273.

[55] Rönnqvist, H. , 2018. Double-ring infiltrometer for in-situ permeability determination of dam material. Engineering, 10(6), 320-328. https://doi.org/10.4236/eng.2018.106022.

[56] Sai Louie, A.J., Morgan, L. K., Banks, E. W., Dempsey, D. and Wilson, S., 2023. Active-distributed temperature sensing dataset beneath a braided river. Data in Brief. 51, p. 109756. https://doi.org/10.1016/j.dib.2023.109756.

[57] Sharma, S.K. and Kennedy, M.D., 2017. Soil aquifer treatment for wastewater treatment and reuse. International Biodeterioration & Biodegradation. 119, pp. 671–677. https://doi.org/10.1016/j.ibiod.2016.09.013.

[58] Silva, G. S. D., Pereira, F. A. D. C., Santana, R. A., Meneses, T. N., LOPES, O. P. and Rosário, A. S. D., 2020. Calibration of a weighing lysimeter for measuring cocoa evapotranspiration. Revista Caatinga, 33(3), 803-814. https://doi.org/10.1590/1983-21252020v33n324rc.

[59] Simon, N., Bour, O., Lavenant, N., Porel, G., Nauleau, B., Pouladi., B., Longuevergne, L. and Crave, A., 2021. Numerical and Experimental Validation of the Applicability of Active-DTS Experiments to Estimate Thermal Conductivity and Groundwater Flux in Porous Media. Water Resources Research. 57(1), p. e2020WR028078. https://doi.org/10.1029/2020WR028078.

[60] Simon, N., Bour, O., Faucheux, M., Lavenant, N., Le Lay, H., Fovet, O., Thomas, Z. and Longuevergne, L., 2022. Combining passive and active distributed temperature sensing measurements to locate and quantify groundwater discharge variability into a headwater stream. Hydrology and Earth System Sciences. 26(5), pp. 1459–1479. https://doi.org/10.5194/hess-26-1459-2022.

[61] Simon, N., Bour, O., Heyman J., Lavenant, N., Petton, C. and Crave, A., 2024. Spatiotemporal Variability of Hyporheic Flow in a Losing River Section. Water Resources Research. 60(6), p. e2023WR035475. https://doi.org/10.1029/2023WR035475.

[62] Simon, N. and Bour, O., 2023. An ADTS Toolbox for Automatically Interpreting Active Distributed Temperature Sensing Measurements. Groundwater. 61(2), pp. 215–223. https://doi.org/10.1111/gwat.13172.

[63] Singh, A., Panda, S. N., Kumar, K. S., Sharma, C. S., 2013. Artificial Groundwater Recharge Zones Mapping Using Remote Sensing and GIS: A Case Study in Indian Punjab. Environmental Management. 52(1), pp. 61–71. https://doi.org/10.1007/s00267-013-0101-1.

[64] Sprenger, C., Hartog, N., Hernandez, M., Vilanova, E., Grützmacher, G., Scheibler, F. and Hannappel, S., 2017. Inventory of managed aquifer recharge sites in Europe: historical development, current situation and perspectives. Hydrogeology Journal. 25(6), pp. 1909–1922. https://doi.org/10.1007/s10040-017-1554-8.

[65] Stauffer, F., Bayer, P., Blum, P., Giraldo, N. M. and Kinzelbach, W., 2013. Thermal Use of Shallow Groundwater (1st ed.). CRC Press. https://doi.org/10.1201/b16239.

[66] Van Cuyk, S., 2001. Hydraulic and purification behaviors and their interactions during wastewater treatment in soil infiltration systems. Water Research. 35(4), pp. 953–964. https://doi.org/10.1016/S0043-1354(00)00349-3.

[67] Wu, W. Y., Lo, M. H., Wada, Y., Famiglietti, J. S., Reager, J. T., Yeh, P. J. F., Ducharme, A. and Yang, Z. L., 2020. Divergent effects of climate change on future groundwater availability in key mid-latitude aquifers. Nature communications, 11(1), 3710.

[68] Young, C.S., 2015. Closed Circuit Television, in *The Science and Technology of Counterterrorism*. Elsevier, pp. 359–418. https://doi.org/10.1016/B978-0-12-420056-2.00011-7.

[69] Zhang, Y., Qian, H., Hou, K., Zhang, Q. and Lin, T., 2024. Evolution of loess-paleosol sequence from the perspectives of thermodynamics and microstructure. Catena, 234, 107627. https://doi.org/10.1016/j.catena.2023.107627.